The true toughness of human cortical bone measured with realistically short cracks

K. J. KOESTER[1], J. W. AGER III[1] AND R. O. RITCHIE[1,2]*

[1]Materials Sciences Division, Lawrence Berkeley National Laboratory, Berkeley, California 94720, USA
[2]Department of Materials Science and Engineering, University of California, Berkeley, California 94720, USA
*e-mail: RORitchie@lbl.gov

Published online: 29 June 2008; doi:10.1038/nmat2221

Bone is more difficult to break than to split. Although this is well known, and many studies exist on the behaviour of long cracks in bone, there is a need for data on the orientation-dependent crack-growth resistance behaviour of human cortical bone that accurately assesses its toughness at appropriate size scales. Here, we use *in situ* mechanical testing to examine how physiologically pertinent short (<600 μm) cracks propagate in both the transverse and longitudinal orientations in cortical bone, using both crack-deflection/twist mechanics and nonlinear-elastic fracture mechanics to determine crack-resistance curves. We find that after only 500 μm of cracking, the driving force for crack propagation was more than five times higher in the transverse (breaking) direction than in the longitudinal (splitting) direction owing to major crack deflections/twists, principally at cement sheaths. Indeed, our results show that the true transverse toughness of cortical bone is far higher than previously reported. However, the toughness in the longitudinal orientation, where cracks tend to follow the cement lines, is quite low at these small crack sizes; it is only when cracks become several millimetres in length that bridging mechanisms can fully develop leading to the (larger-crack) toughnesses generally quoted for bone.

Bone is a complex hierarchical composite of collagen and hydroxyapatite that is imbued with mechanisms to resist fracture at different size scales[1]. These size scales relate to the characteristic structural dimensions in bone, which vary from twisted peptide chains at the nanoscale, hydroxyapatite-impregnated twisted collagen fibrils at the scale of tens of nanometres, collagen fibres that are typically a micrometre in diameter, the lamellar structure of collagen fibres at micrometre dimensions, to the (secondary) osteon (haversian) structures, which are several hundred micrometres in size. It is the simultaneous operation of toughening mechanisms at these various length scales that provides bone with its enduring strength and toughness. However, as the mechanical properties of bone can undergo deleterious changes with ageing[2,3] and disease[4], it is imperative to understand, both quantitatively and mechanistically, the origins of its fracture resistance to develop therapies to inhibit or reverse these negative effects.

There are complications with this approach though when applied to human bone. Cortical bone develops its toughness primarily from extrinsic mechanisms during crack growth, as opposed to intrinsic mechanisms that are more associated with crack initiation[3,5,6]. Fracture can be thought of as a mutual competition between intrinsic damage mechanisms, which operate ahead of the crack tip to promote cracking, and extrinsic toughening mechanisms, which act primarily in the crack wake to 'shield' the crack from the applied driving force to inhibit cracking. Extrinsic toughening, which is most relevant for brittle materials (including bone), invariably results in resistance-curve behaviour, that is, the need for a progressively increasing applied driving force to sustain crack extension[7]. As bone's fracture behaviour is intimately coupled to its hierarchical structure, the measured toughness can be a function of the size scale at which it is assessed. In addition, measurements need to reflect cracking behaviour in the more clinically relevant transverse orientation, that is, to break rather than split bone, and involve realistic flaw sizes pertinent to human bones. Accordingly, we have attempted to measure, for the first time, crack-resistance curves (*R*-curves) for human cortical bone in the transverse orientation, using *in situ* measurements/observations in an environmental scanning electron microscope (ESEM), coupled with fractographic and synchrotron X-ray computed tomography studies to identify the salient damage and toughening mechanisms. Our approach is threefold: we use nonlinear-elastic fracture mechanics, with crack-deflection mechanics, to properly quantify the toughness properties, we have examined both crack-initiation and crack-growth (*R*-curve) toughnesses for realistically short crack sizes and we have compared behaviour with the more commonly evaluated longitudinal orientation.

There have of course been numerous previous evaluations of the toughness of mammalian cortical bone (Table 1)[2,8–20], although none has focused on evaluating the important crack-growth properties for the short crack sizes associated with the cortical shell in the transverse orientation. Indeed, most previous measurements have involved single-value characterizations of the toughness[8–20], for example, the fracture toughness K_c, which do not necessarily include any contribution from the crack-growth toughness; moreover, such measurements have, with few exceptions[2,19,20], been based on linear-elastic fracture mechanics[8–19], which minimizes any contribution from plastic (inelastic) deformation, or have involved large crack sizes (~several millimetres) in the longitudinal orientations (where it is easier to make measurements). There have been crack-growth resistance measurements[3,6,21] (although none in human cortical bone in the transverse orientation) that have identified several microscale toughening mechanisms, including viscoplastic flow[22], microcracking[5,23,24], crack deflection[25–27] and crack bridging[21,28,29]. Despite this body of research, there are

Table 1 Single-value toughness measurements of mammalian cortical bone in the longitudinal and transverse orientations[2,8–20]. SENT: single-edged notched tension; SENB: single-edged notched bend; C(T): compact tension.

Bone	Orientation	K_c (MPa m$^{1/2}$)	Geometry	Authors	Year
Bovine femur	Longitudinal	3.21	SENT	Melvin and Evans[8]	1973
Bovine femur	Transverse	5.6	SENT	Melvin and Evans[8]	1973
Bovine femur	Transverse	2.2–4.6	SENT	Bonfield and Datta[9]	1976
Bovine femur	Longitudinal	3.62	C(T)	Wright and Hayes[10]	1977
Bovine femur	Longitudinal	2.4–5.2	C(T)	Bonfield *et al.*[11]	1978
Bovine tibia	Longitudinal	2.8	C(T)	Behiri and Bonfield[12]	1984
Human tibia	Longitudinal	2.4–5.3	C(T)	Behiri and Bonfield[12]	1984
Bovine tibia	Transverse	11.2	SENB	Moyle and Gavens[13]	1986
Human tibia	Longitudinal	3.7	C(T)	Norman *et al.*[14]	1991
Bovine tibia	Longitudinal	7.2	C(T)	Norman *et al.*[14]	1991
Bovine tibia	Longitudinal	6.2–6.7	C(T)	Norman *et al.*[15]	1995
Human femur	Transverse	6.4	SENB	Zioupos and Currey[2]	1997
Bovine femur	Longitudinal	4.9	CNT	De Santis[16]	2000
Baboon femur	Longitudinal	1.8	C(T)	Phelps *et al.*[17]	2000
Baboon femur	Transverse	6.2	SENB	Phelps *et al.*[17]	2000
Human femur	Longitudinal	5.1	SENB	Wang *et al.*[18]	2002
Equine metatarsal	Transverse	6.0–9.0	C(T)†	Malik *et al.*[19]	2003
Bovine femur	Longitudinal	2.6	C(T)†	Yan *et al.*[20]	2007
Bovine femur	Transverse	5.1	C(T)†	Yan *et al.*[20]	2007
Bovine femur	Longitudinal	6.2*	C(T)†	Yan *et al.*[20]	2007
Bovine Femur	Transverse	10.5*	C(T)†	Yan *et al.*[20]	2007

*Denotes a value of K_c back-calculated from J_c.

†Denotes side-grooved specimens.

still critical issues that remain to be assessed, namely that of the true crack-growth resistance of human cortical bone at physiologically relevant short crack sizes, how this specifically changes with orientation and a mechanistic understanding of the microstructural damage and toughening mechanisms involved.

Here, we use nonlinear-elastic fracture mechanics testing of human cortical bone under hydrated conditions *in situ* in an ESEM to permit resistance-curve measurements for growing short cracks, less than ~1,000 μm in size, in both the transverse and longitudinal (proximal–distal) orientations, with simultaneous high-resolution imaging of crack paths to discern the dominant sources of toughness and to show how they actually confer crack-growth resistance. Our focus is on the transverse orientation because this is often the more clinically relevant direction[1,30]; however, cracks growing in this orientation invariably deflect along the longitudinal direction such that both orientations act in concert to provide resistance to fracture.

Using test samples from the midsection of the frozen caderveric humeral cortical bone of three 37–41-year-old donors, both single-edged notched bend and compact-tension samples were sectioned and notched from locations longitudinal or transverse to the bone long axis. The notch orientation was such that the nominal crack-growth direction was either along the proximal–distal direction of the humerus, in the longitudinal–radial plane, that is, parallel to the long axis of the osteons (longitudinal), or transverse to the long axis of the humerus (transverse), as in Fig. 1. We monitored stable crack extensions ($\Delta a < 1{,}000$ μm) in three-point bend samples soaked in Hanks' balanced salt solution (HBSS), *in situ* in the ESEM, and extra bend and compact-tension samples *ex situ* (outside the ESEM) in HBSS, all at 25 °C, to obtain information for larger crack extensions ($\Delta a \sim 150$–$7{,}000$ μm); the results are presented in terms of measurements of the crack-driving force, specifically the stress-intensity factor K and J-integral. (Under nonlinear-elastic conditions, that is, in the presence of some degree of inelasticity (for example, plastic deformation), the fracture toughness is better described in terms of the J-integral, which characterizes the corresponding distribution of local inelastic stresses and displacements at the crack tip[31], see the Methods section).

Our results showing the increase in crack-driving force as a function of crack extension, that is, the $K(\Delta a)$ resistance curves, for human cortical bone, are shown in Fig. 1, with simultaneous images of the crack profiles in Fig. 2. This is the first time that nonlinear-elastic fracture mechanics has been used to analyse the crack-resistance curve behaviour of physiologically relevant short cracks in human bone. The degree of toughening in the transverse orientation is very large, concomitant with gross crack deflection/twisting/meandering/delamination along the longitudinal and circumferential directions, which results in extremely rough fracture surfaces (Fig. 2a–e). Stress intensities for crack extension reach values of 25 MPa m$^{1/2}$ ($J \sim 31$ kJ m^{-2}) over the first 500 μm of cracking, representing toughness values much higher than have previously been reported (Table 1). In contrast, corresponding fracture in the longitudinal orientation requires far lower driving forces, specifically, stress intensities between 1 and 2 MPa m$^{1/2}$ ($J \sim 0.05$–0.2 kJ m^{-2}) to initially extend the crack the first ~500 μm, consistent with the highly linear crack profiles and smooth fracture surfaces (Fig. 2f,j); however, with continued crack extension into the millimetre range, toughness values approach 5 MPa m$^{1/2}$ ($J \sim 1.2$ kJ m^{-2}), consistent with K_c values measured in most previous studies (see Table 1). We note here that the short-crack K values of ~1–2 MPa m$^{1/2}$ for initial longitudinal crack propagation, although seemingly quite low, are consistent with a recent study of short-crack R-curve behaviour, by Mullins *et al.*[32], who report values of 0.5–2.3 MPa m$^{1/2}$ for 5 to 60 μm cracks in this orientation emanating from hardness indentations in ovine bone. We further note that our R-curve/toughness values in Fig. 1 are relatively insensitive to (1) changes in displacement rate, which was varied from 0.04 to 6 μm s^{-1}, (2) any differences in hydration of our bone samples caused by the *in situ* loading of HBSS-saturated specimens within the ESEM versus the *ex situ* loading of specimens immersed in HBSS and (3) any loss of constraint due to the small size of our *in situ* bend samples (further tests with a 7.5-mm-thick specimen

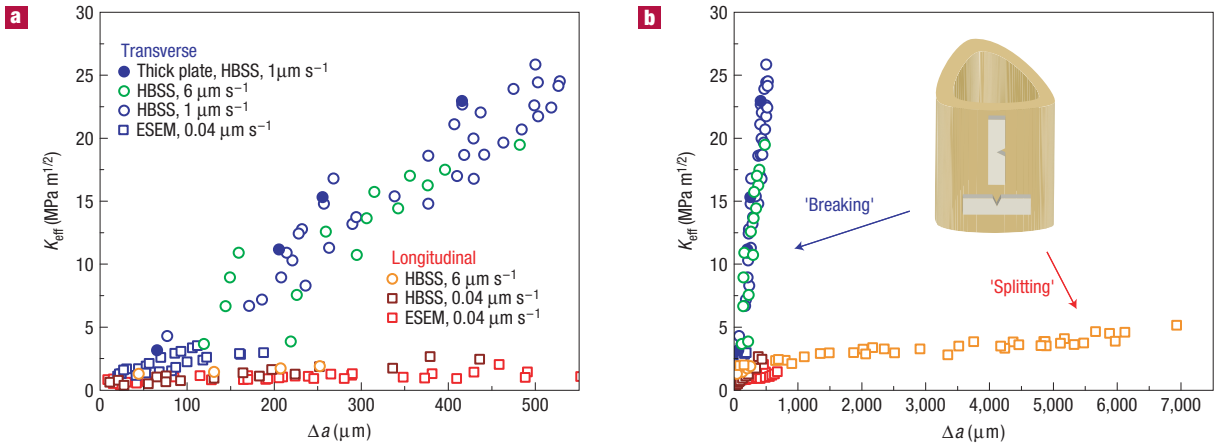

Figure 1 Crack-resistance curves (*R*-curves) showing the orientation and crack-size-dependent fracture resistance for human cortical bone measured at different strain rates and hydration levels. K_{eff} is defined in equation (2). **a**,**b**, *R*-curves for short crack lengths ($\Delta a < 550\,\mu m$) (**a**) and combined with longer-crack ($\Delta a < 7{,}000\,\mu m$) *R*-curves (**b**). In the legend, ESEM denotes testing *in situ* in the ESEM and HBSS denotes testing *ex situ* immersed in HBSS; individual displacement rates are also given. The inset shows the orientation of the samples from the humerus. It is clear from the plots that bone principally derives its toughness during through-crack growth, rather than crack initiation; moreover, such resistance to crack growth increases much more rapidly in the transverse direction than in the longitudinal direction, resulting in crack-growth toughnesses exceeding 20 MPa $m^{1/2}$. This was found to be the result of different toughening mechanisms in each orientation, specifically, crack deflection and twist in the transverse orientation and crack bridging in the longitudinal orientation. It was verified that this was not an effect of hydration, displacement rate or loss of constraint; *in situ* and *ex situ* measurements of *R*-curves at different displacement rates, and with a thick-plate sample, did not affect the *R*-curve data for either orientation.

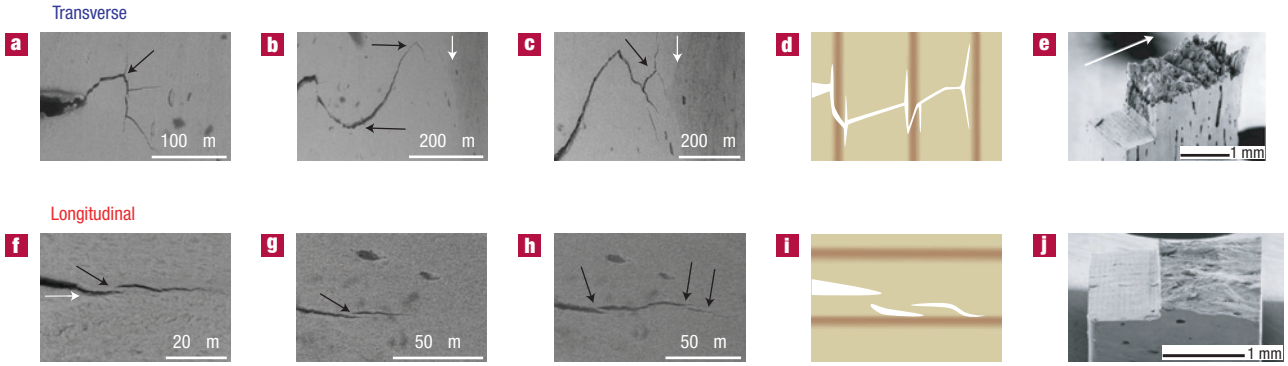

Figure 2 Crack profiles, schematic diagrams and fractography of the different extrinsic toughening mechanisms in the transverse and longitudinal orientations. **a**–**j**, Crack profiles for representative cracks, for three different crack lengths, in the transverse ('breaking') (**a**–**c**) and longitudinal ('splitting') (**f**–**h**) directions and an ESEM fractography image (**e**,**j**) and a schematic diagram (**d**,**i**) of the crack trajectory for each orientation. In **a**–**c**, the black arrows indicate the major in-plane deflections of the crack and the white arrows indicate the cement sheath. It can be seen from **a**–**c** that cracks in the transverse direction undergo multiple in-plane deflections, which in conjunction with the through-thickness twists (see Fig. 3 and the end of the transverse video in the Supplementary Information), give rise to the rough fracture surface in **e**. A schematic diagram of the crack profile is shown in **d**, where the crack deflects at the cement sheaths as it propagates through the haversian bone. In **f**–**h**, the black arrows indicate the formation of uncracked-ligament bridges, and the white arrow in **f** indicates the cement sheath. In contrast to the transverse direction, in the longitudinal direction, the cracks do not deflect at the cement sheaths but follow them; this gives rise to a relatively flat fracture surface (**j**). At the cement sheaths in this orientation, it is common for a new crack to initiate ahead of the propagating crack, resulting in the so-called 'mother–daughter' crack configuration[44] and the consequent formation of bridges, as shown schematically in **i**. The area fraction and size of these bridges was found to be dependent on crack size, with the toughening effect of bridging becoming more prominent with longer crack extensions.

gave a similar transverse *R*-curve to the bulk of our data, which were determined with 1.5-mm-thick specimens).

The specific damage and toughening mechanisms associated with this behaviour were imaged in real time through the use of *in situ* electron microscopy. We find that crack trajectories are highly deflected, both in-plane and out-of-plane (crack twist), in the transverse orientation and relatively linear in the longitudinal direction (Figs 2,3). Specifically, for the transverse direction, cracks tend in general to deflect away from the nominal mode-I plane, that is, the plane of maximum tensile (tangential) stress, governed by a $K_{II} = 0$ path, and then periodically to 'delaminate' along internal interfaces, involving deflections of ~90° for tens to hundreds of

micrometres, in the longitudinal direction, before reinitiating at a much higher applied load and continuing their deflected path along the (nominal) transverse direction; this process is repeated several times throughout the cortical bone specimen. In contrast, crack paths in the longitudinal direction remain comparatively linear along the nominal mode-I plane, although multiple (overlapping) cracks are generated with (microscopic) 'uncracked ligaments', some tens of micrometres in size, in between. Such uncracked regions are the source of crack bridging in bone, but are only fully developed as crack extension proceeds into the millimetre range.

Of particular note for these differing fracture paths is that surrounding the major cracks, there is clear evidence of microcracking, that is, smaller cracks typically tens of micrometres in length, within the bone matrix[33,34]. These microcracks are primarily orientated along the longitudinal direction; they are therefore roughly parallel to the primary crack path in longitudinal specimens and perpendicular in transverse specimens (Fig. 2). Such microcracks form at 'weak links' in the bone-matrix structure; they occur primarily along cement sheaths, that is, at the refractile boundaries of the haversian systems (secondary osteons), and to a lesser extent at lamellar interfaces[35], and correspondingly have a typical spacing in the tens to hundreds of micrometres range aligned along the long axis of the bone.

We find that the formation of these microcracks, and specifically their orientation, are essential to the orientation-dependent fracture toughness of cortical bone; indeed, their presence forms the basis of the contrasting toughening behaviour in the two orientations. In the transverse orientation, the microcracks at the cement lines are roughly aligned perpendicular to the crack path, where they act as 'delamination barriers' (through the Cook–Gordon mechanism of crack arrest at weak interfaces[36]); this serves to blunt the crack, cause crack deflections of ~90°, generate highly tortuous crack paths (Fig. 2a–d), yield extremely rough fracture surfaces (Fig. 2e) and correspondingly high toughness. The last of these follows because of the reduced local stress field due to blunting and the need to reinitiate the crack following perpendicular delaminations; in addition, such gross crack-path deviations away from the plane of maximum tensile stress greatly diminish the local stress intensity at the crack tip, thereby necessitating higher applied loads to continue cracking.

Conversely, in the longitudinal orientation, the microcracks are aligned roughly parallel to the growing crack; their formation alongside and ahead of the crack tip is the precursor to the formation of so-called 'uncracked-ligament' bridges, which toughen by resisting the opening of the crack[28]. However, we do not believe that the microcracks *per se* toughen the material, through a constrained microcracking mechanism, that is, where the dilation associated with microcracks formed around a crack is constrained by surrounding material, thereby putting the crack in compression[37]. Calculations suggest that the contribution to the toughness of cortical bone from this mechanism is relatively small[38]. The vital role of microcracks is to induce both primary forms of toughening in bone, that of crack deflection and crack bridging.

These observations of contrasting nature of damage and toughening in the transverse and longitudinal orientation are summarized in Fig. 2d,i) and in the movies in the Supplementary Information. However, as they are based on *in situ* ESEM observations, they reflect the surface cracking behaviour. To discern what is happening below the surface, we used synchrotron X-ray computed tomography to image the underlying structure of the bone and to determine how the cracks interact with this structure. Specifically, three-dimensional images of crack propagation in the transverse orientation, together with two-dimensional slices showing the crack at different depths throughout the sample, show the major crack-deflections/twists as the crack encounters the osteons (Fig. 3). Although the frequency of these major deflections seems in two-dimensional slices to be in the tens of micrometres range, it is clear from three-dimensional imaging that this is

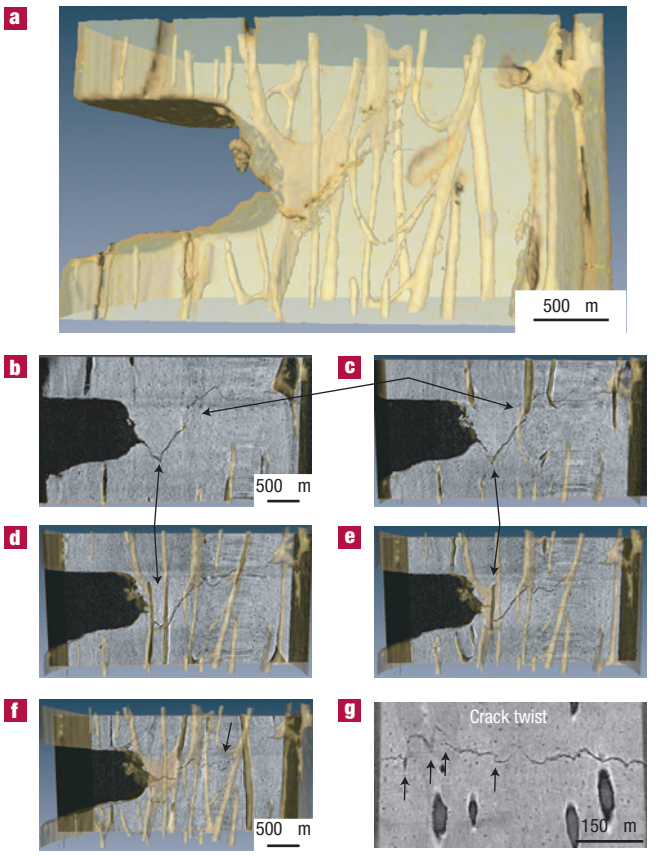

Figure 3 Synchrotron X-ray computed tomography images showing the dominant mechanisms of crack deflection and twisting in the transverse orientation. Toughening in human bone is most prominent in the transverse ('breaking') orientation, where the crack undergoes marked deflections and (out-of-plane) twists as it interacts with the underlying haversian structure. **a**, A three-dimensional reconstruction of the sample in which the haversian canals are partially transparent. **b–f**, A series of tomographic slices through the thickness of the sample combined with the transparent three-dimensional reconstruction of the sample, starting with the front face in **b** and moving to the back face in **f**, at depths of 289 μm (**b**), 342 μm (**c**), 387 μm (**d**), 507 μm (**e**) and 587 μm (**f**). In **b–f**, the arrows indicate the in-plane deflections and the associated underlying haversian systems. The arrow connecting the features in **b** and **c** shows that the ~90° deflection of the crack is related to a haversian system at a greater depth; the initial downward deflection of the crack as it grew off the notch is related to the three haversian systems deeper in the sample. Interestingly, this deflection is even sharper in the plane of the haversian canal, as shown in **e**. In **f**, it can be seen that the crack has a markedly different trajectory and undergoes multiple in-plane deflections for shorter distances, as indicated by the arrow. **g**, A through-thickness slice from the front face to the back face near the crack tip highlighting the twist of the crack through the sample. The arrows indicate the major twists, ~90°; it can be seen that in addition to the twists of this magnitude, the crack twists through the entire thickness at lower angles. This combination of in-plane deflections and through-thickness twists is related to the haversian structure of bone and gives rise to the rough fracture surface in Fig. 2e and is a dominant source of the high fracture resistance and crack-growth toughness exceeding 20 MPa $m^{1/2}$, as reported in Fig. 1.

controlled not by the in-plane spacing of the haversian systems (~ hundreds of micrometres), but by the spacing of the haversian systems at different depths through the sample. If the haversian systems from the three-dimensional imaging are projected onto a single plane, their spacing coincides with the frequency of these major deflections. Also of significance is that these three-dimensional images show that such crack deflection involves twisting of the crack, in addition to the in-plane tilts.

The importance of the short-crack (<500 μm) toughness properties cannot be overstated. For example, because the midshaft cortical shell of the humerus is only ~3–5 mm thick, it is unlikely that data on stable crack growth of the order of millimetres would be very relevant to *in vivo* fracture. Moreover, parallel studies on dentin have shown that dominant toughening mechanisms identified at large crack sizes (up to 6 mm) do not necessarily reflect the physiologically relevant fracture behaviour of human tooth dentin where crack sizes are so much smaller (in the tens to hundreds of micrometres range)[39]. For the present measurements on bone, crack-initiation toughnesses, that is, where $\Delta a \rightarrow 0$, are comparable for both orientations (~1 MPa $m^{1/2}$). With further crack extension, the crack-growth resistance will begin to increase as the scale of the relevant toughening mechanisms is encountered. In the longitudinal orientation, the toughness of 1–2 MPa $m^{1/2}$ in the short-crack (<500 μm) regime essentially reflects the toughness of the cement sheaths; further crack extension into the millimetre range is required before significant uncracked-ligament bridges can develop such that the toughness approaches more expected values ~5 MPa $m^{1/2}$. In the transverse orientation, the characteristic size scale pertains to the spacing of the osteons, which controls the process of crack deflection and twist at the cement lines; cracks must only extend ~100 μm or so to activate this mechanism to cause rising *R*-curve behaviour.

This process of major crack deflections at cement sheaths is clearly the most potent toughening mechanism in cortical bone. As noted above, three-dimensional tomographic imaging (Fig. 3) reveals extensive twisting of the crack path, in addition to in-plane (~90°) deflections, which substantially enhances the degree of toughening. Quantitatively, this toughening can be estimated using crack-deflection mechanics. The local mode-I and -II linear-elastic stress intensities, k_1 and k_2, at the tip of a deflected crack, can be stated in terms of the applied stress intensities, K_I and K_{II}, by[40]:

$$k_1 = c_{11}(\alpha)K_I + c_{12}(\alpha)K_{II} \quad \text{and} \quad k_2 = c_{21}(\alpha)K_I + c_{22}(\alpha)K_{II}, \tag{1}$$

where $c_{ij}(\alpha)$ are mathematical functions of the deflection angle α. From equation (1), it can be calculated that one simple in-plane crack deflection by $\alpha \sim 90°$ can reduce the stress intensity at the crack tip by roughly a factor of two, thereby effectively doubling the fracture toughness[38]. However, if we now incorporate crack twisting, the effect is much larger. The local stress intensities that result from the twisting of a deflected crack can be calculated by using crack-twist mechanics, where the effective local mode-I and -III stress intensities at the tip of the twisted and deflected crack are given by[41]:

$$k_I^{tw} = c_{11}(\phi)k_I + c_{12}(\phi)k_{II} \quad \text{and} \quad k_{III}^{tw} = c_{31}(\phi)k_I + c_{32}(\phi)k_{II},$$

where $c_{ij}(\phi)$ are mathematical functions of the twist angle ϕ and k_I and k_{II} are given in equation (1). Any combination of a twist of 45° and a deflection of 45° can halve the crack-tip stress intensity; however, a twist of 45° and a deflection of 90°, which is typical of transverse crack propagation in bone (Fig. 3), decreases the stress intensity at the crack tip by a factor of six. Accordingly, it is clear that such combinations of twist and deflection can lead to significant toughening in human bone, by factors of the order of two to six. Indeed, if these mechanisms are suppressed, for example, by using side-grooved test samples, measured toughness will be much lower (see ref. 20). These toughening mechanisms are consistent with the very rapid increase in crack-growth resistance in the transverse orientation (Figs 1,3) and are undoubtedly why bone is much more difficult to break than to split.

METHODS

SAMPLE PREPARATION

Test samples from the midsection of frozen caderveric humeral cortical bone were wet sectioned using a low-speed saw and machined into seventeen 1.5-mm-thick, 8-mm-long bend samples (width $W = 2$ mm) and five 1.2–3.3-mm-thick compact-tension samples ($W = 13$–18 mm). Samples were then taken from locations longitudinal or transverse to the bone long axis, and notched to form an initial crack of roughly half the sample width, which was then sharpened with a micronotching technique using a razor blade irrigated with a 1 μm diamond suspension. The orientation of the notch was such that the nominal crack-growth direction was either along the proximal–distal direction in the longitudinal–radial plane (longitudinal orientation) or transverse to the long axis of the humerus (transverse orientation). All samples were wet polished with an increasingly higher finish to a final polish with a 0.05 μm diamond suspension before being immersed in ambient HBSS for 4–24 h before testing.

FRACTURE TOUGHNESS/ *R*-CURVE MEASUREMENTS

In situ testing of samples soaked in HBSS was carried out for stable crack extensions less than ~600 μm for the longitudinal orientation and ~150 μm in the transverse orientation in a Hitachi S-4300SE/N ESEM (Hitachi America) at 25 °C using a Gatan Microtest 2kN three-point bending stage (Gatan); images of the crack path were obtained simultaneously in backscattering mode at 15 kV and a pressure of 35 Pa. In addition, we tested samples *ex situ* in HBSS at 25 °C on an EnduraTec Elf 3200 testing machine (BOSE) and an MTS 810 (MTS Corporation) to determine the *R*-curve for larger crack extensions ($\Delta a \sim$ 150–7,000 μm).

Fracture toughness *R*-curves were determined in terms of the crack-driving force as a function of crack extension (Δa). Where crack paths remained relatively linear and did not undergo large deflections, that is, they extended approximately along the expected path of the maximum tensile stress, as for most samples tested in the longitudinal orientation, standard handbook linear-elastic mode-I solutions for cracks in these geometries[42] were used to obtain the stress intensity. For samples tested in the transverse orientation, conversely, cracks grew at an angle to the mode-I plane (of maximum tensile stress). Such crack deflection induces mixed-load loading at the crack tip, that is, mode-I (tensile opening) plus mode-II (shear), such that standard mode-I stress intensity solutions are not applicable. For the first 100–200 μm of crack extension, the cracks grew away from the notch at a constant angle such that standard crack deflection solutions[40] could be used to compute a mixed-mode driving force, as has been done in human dentin[39]. With further crack extension in the transverse orientation, cracks often deflected several times. To determine the *R*-curve for these more complex crack paths, a nonlinear-elastic fracture mechanics approach was used in which the crack-driving force was calculated using the *J*-integral[42] and crack lengths were estimated in terms of the equivalent through-thickness crack with the same compliance. (Typically, for a deflected crack with a total length of 850 μm, where the projected length along the nominal mode-I plane would be of the order of 625 μm, the computed length of the linear crack with equivalence compliance would be in between these values, within ~10% of the total length). This approach accounts for the contribution from plasticity (inelasticity in bone) to the toughness, and provides a sound means to determine the *R*-curve fracture toughness in a material that undergoes multiple large-scale crack deflections; moreover, the *J*-integral is much more suitable than the stress intensity to characterize the toughness under mixed-mode fracture conditions. To monitor crack extension, measurements of the elastic compliance, C_{LL}, were made during periodic unloading (~10%) every ~25 μm of crack extension during the *R*-curve test. The relationship between C_{LL} and the equivalent through-thickness crack length, *a*, was obtained from handbook solutions[42]. The stress intensity at each measured crack length was calculated by measuring the nonlinear strain-energy release rate, *J*, where *J* is defined as the rate of change in potential energy under nonlinear-elastic conditions for a unit increase in crack area[43], which is

equivalent to G under elastic conditions. J can be determined in terms of the sum of its elastic and plastic contributions:

$$J = J_{el} + J_{pl}.$$

The plastic component of J was calculated from[42]

$$J_{pl} = \frac{2A_{pl}}{Bb},$$

where A_{pl} is the area under the plastic region of the load versus load-point displacement curve, B is the specimen thickness and b is the (macroscopic) uncracked ligament $(W - a)$; the corresponding elastic component given by $J_{el} = K^2/E'$ was small and typically only 5–10% of J_{pl}. However, because it is unusual to express the toughness of biological materials such as bone in terms of J, equivalent (effective) stress intensities were then computed from the standard J–K equivalence (mode I) relationship:

$$K_{eff} = \sqrt{JE}, \quad (2)$$

with the Young's modulus for bone taken as $E = 20$ GPa. This is the toughness parameter that is plotted in Fig. 1.

We believe that the approach used here is necessary for a full understanding of the fracture properties of human cortical bone: we have examined realistic short cracks in both the longitudinal and transverse orientations, used an R-curve analysis to capture both crack initiation and growth behaviour, accounted for the inelasticity and mixed-mode loading using the J-integral and simultaneously characterized the development of the extrinsic toughening mechanisms in cortical bone.

Received 4 April 2008; accepted 19 May 2008; published 29 June 2008.

References

1. Currey, J. D. *Bones* (Princeton Univ. Press, Princeton, 2002).
2. Zioupos, P. & Currey, J. D. Changes in the stiffness, strength, and toughness of human cortical bone with age. *Bone* **22**, 57–66 (1998).
3. Nalla, R. K., Kruzic, J. J., Kinney, J. H. & Ritchie, R. O. Effect of aging on the toughness of human cortical bone: Evaluation by *R*-curves. *Bone* **35**, 1240–1246 (2004).
4. Giannoudis, P., Tzioupis, C., Almalki, T. & Buckley, R. Fracture healing in osteoporotic fractures: Is it really different? A basic science perspective. *Injury Sci. Basis Fracture Healing: An Update* **38**, S90–S99 (2007).
5. Vashishth, D., Tanner, K. E. & Bonfield, W. Experimental validation of a microcracking-based toughening mechanism for cortical bone. *J. Biomech.* **36**, 121–124 (2003).
6. Vashishth, D. Rising crack-growth-resistance behavior in cortical bone: Implications for toughness measurements. *J. Biomech.* **37**, 943–946 (2004).
7. Ritchie, R. O., Gilbert, C. J. & McNaney, J. M. Mechanics and mechanisms of fatigue damage and crack growth in advanced materials. *Int. J. Solids Struct.* **37**, 311–329 (2000).
8. Melvin, J. W. & Evans, F. G. *Biomechanics Symp.* 87–88 (ASME, New York, 1973).
9. Bonfield, W. & Datta, P. K. Fracture toughness of compact bone. *J. Biomech.* **9**, 131–134 (1976).
10. Wright, T. M. & Hayes, W. C. Fracture mechanics parameters for compact bone–effects of density and specimen thickness. *J. Biomech.* **10**, 419–425 (1977).
11. Bonfield, W., Grynpas, M. D. & Young, R. J. Crack velocity and the fracture of bone. *J. Biomech.* **11**, 473–479 (1978).
12. Behiri, J. C. & Bonfield, W. Fracture mechanics of bone–the effects of density, specimen thickness and crack velocity on longitudinal fracture. *J. Biomech.* **17**, 25–34 (1984).
13. Moyle, D. D. & Gavens, A. J. Fracture properties of bovine tibial bone. *J. Biomech.* **19**, 919–927 (1986).
14. Norman, T. L., Vashishth, D. & Burr, D. B. in *Advances in Bioengineering* Vol. 20 (ed. Vanerby, R.) 361–364 (ASME, New York, 1991).
15. Norman, T. L., Vashishth, D. & Burr, D. B. Fracture toughness of human bone under tension. *J. Biomech.* **28**, 309–320 (1995).
16. De Santis, R. *et al.* Bone fracture analysis on the short rod chevron-notch specimens using the x-ray computer micro-tomography. *J. Mater. Sci. - Mater. Med.* **11**, 629–636 (2000).
17. Phelps, J. B., Hubbard, G. B., Wang, X. & Agrawal, C. M. Microstructural heterogeneity and the fracture toughness of bone. *J. Biomed. Mater. Res.* **51**, 735–741 (2000).
18. Wang, X., Shen, X., Li, X. & Mauli Agrawal, C. Age-related changes in the collagen network and toughness of bone. *Bone* **31**, 1–7 (2002).
19. Malik, C. L., Stover, S. M., Martin, R. B. & Gibeling, J. C. Equine cortical bone exhibits rising *R*-curve fracture mechanics. *J. Biomech.* **36**, 191–198 (2003).
20. Yan, J., Mecholsky, J., John, J. & Clifton, K. B. How tough is bone? Application of elastic–plastic fracture mechanics to bone. *Bone* **40**, 479–484 (2007).
21. Nalla, R. K., Kruzic, J. J., Kinney, J. H. & Ritchie, R. O. Mechanistic aspects of fracture and *R*-curve behavior in human cortical bone. *Biomaterials* **26**, 217–231 (2005).
22. Fantner, G. *et al.* Sacrificial bonds and hidden length dissipate energy as mineralized fibrils separate during bone fracture. *Nature Mater.* **4**, 612–616 (2005).
23. Vashishth, D., Behiri, J. C. & Bonfield, W. Crack growth resistance in cortical bone: Concept of microcrack toughening. *J. Biomech.* **30**, 763–769 (1997).
24. Vashishth, D. Rising crack-growth-resistance behavior in cortical bone: Implications for toughness measurements. *J. Biomech.* **37**, 943–946 (2004).
25. Brown, C. U., Yeni, Y. N. & Norman, T. L. Fracture toughness is dependent on bone location—a study of the femoral neck, femoral shaft, and the tibial shaft. *J. Biomed. Mater. Res.* **49**, 380–389 (2000).
26. Parasamian, G. & Norman, T. Diffuse damage accumulation in the fracture process zone of human cortical bone specimens and its influence on fracture toughness. *J. Mater. Sci. - Mater. Med.* **12**, 779–783 (2001).
27. Peterlik, H., Roschger, P., Klaushoffer, K. & Fratzl, P. From brittle to ductile fracture of bone. *Nature Mater.* **5**, 52–55 (2006).
28. Nalla, R. K., Kinney, J. H. & Ritchie, R. O. Mechanistic fracture criteria for the failure of human cortical bone. *Nature Mater.* **2**, 164–168 (2003).
29. Yeni, Y. N. & Fyhrie, D. P. A rate-dependent microcrack-bridging model that can explain the strain rate dependency of cortical bone apparent yield strength. *J. Biomech.* **36**, 1343–1353 (2003).
30. Behiri, J. C. & Bonfield, W. Orientation dependence of the fracture mechanics of cortical bone. *J. Biomech.* **22**, 863–867 (1989).
31. Knott, J. F. *Fundamentals of Fracture Mechanics* (Butterworth & Co., London, 1976).
32. Mullins, L., Bruzzi, M. & McHugh, P. Measurement of microstructural fracture toughness of cortical bone using indentation toughness. *J. Biomech.* **40**, 3285–3288 (2007).
33. Burr, D. B. & Martin, R. B. Calculating the probability that microcracks initiate resorption spaces. *J. Biomech.* **26**, 613–616 (1993).
34. Taylor, D., Hazenberg, J. G. & Lee, T. C. Living with cracks: Damage and repair in human bone. *Nature Mater.* **6**, 249–317 (2007).
35. Yeni, Y. & Norman, T. L. Calculation of porosity and osteonal cement line effects on the effective fracture toughness of cortical bone in longitudinal crack growth. *J. Biomed. Mater. Res.* **51**, 504–509 (2000).
36. Cook, J., Gordon, J. E., Evans, C. C. & Marsh, D. M. A mechanism for the control of crack propagation in all-brittle systems. *Proc. R. Soc. Lond. A* **282**, 508–520 (1964).
37. Evans, A. G. & Faber, K. T. Crack-growth resistance of microcracking brittle materials. *J. Am. Ceram. Soc.* **67**, 255–260 (1984).
38. Nalla, R. K., Stölken, J. S., Kinney, J. H. & Ritchie, R. O. Fracture in human cortical bone: Local fracture criteria and toughening mechanisms. *J. Biomech.* **38**, 1517–1525 (2005).
39. Koester, K. J., Ager, J. W. III & Ritchie, R. O. The effect of aging on crack-growth resistance and toughening mechanisms in human dentin. *Biomaterials* **29**, 1318–1328 (2008).
40. Cotterell, B. & Rice, J. R. Slightly curved or kinked cracks. *Int. J. Fract.* **16**, 155–169 (1980).
41. Faber, K. T. & Evans, A. G. Crack deflection process—I theory. *Acta Metall.* **31**, 565–576 (1983).
42. E1820, *Standard test method for measurement of fracture toughness* (American Society for Testing and Materials, West Conshohocken, PA, 2006).
43. Rice, J. R. A path independent integral and the approximate analysis of strain concentration by notches and cracks. *J. Appl. Mech.* **35**, 379–386 (1968).
44. Yang, Q. D., Cox, B. N., Nalla, R. K. & Ritchie, R. O. Re-evaluating the toughness of human cortical bone. *Bone* **38**, 878–887 (2006).

Supplementary Information accompanies this paper on www.nature.com/naturematerials.

Acknowledgements

This work was supported by the Director, Office of Science, Office of Basic Energy Sciences, Division of Materials Sciences and Engineering, of the US Department of Energy under contract no. DE-AC02-05CH11231, and by the Laboratory Directed Research and Development Program of Lawrence Berkeley National Laboratory (LBNL). Computed X-ray tomography was carried out at LBNL's Advanced Light Source, which is supported under the same contract. The authors thank H. Barth for help in preparing the X-ray computed tomographs.

Author contributions

R.O.R. had full access to the experimental data in the study and takes responsibility for the integrity of the data and the accuracy of the data analysis. Data acquisition was carried out by K.J.K. Study design, interpretation and analysis of data and preparation of the manuscript were performed jointly by K.J.K., J.W.A. and R.O.R.

Author information

Reprints and permission information is available online at http://npg.nature.com/reprintsandpermissions.
Correspondence and requests for materials should be addressed to R.O.R.